*Journal of The Electrochemical Society*, **158** (4) A363-A370 (2011)
0013-4651/2011/158(4)/A363/8/$28.00 © The Electrochemical Society


# Kinetic Monte Carlo Simulation of Surface Heterogeneity in Graphite Anodes for Lithium-Ion Batteries: Passive Layer Formation

**Ravi N. Methekar,[a,*] Paul W. C. Northrop,[a] Kejia Chen,[b] Richard D. Braatz,[b] and Venkat R. Subramanian[a,**,z]**

[a]*Department of Energy, Environmental and Chemical Engineering, Washington University, Saint Louis, Missouri 63130, USA*
[b]*Chemical and Biomolecular Engineering, University of Illinois at Urbana-Champaign, Urbana, Illinois 61801, USA*

The properties and chemical composition of the solid-electrolyte-interface (SEI) layer have been a subject of intense research due to their importance in the safety, capacity fade, and cycle life of Li-ion secondary batteries. In this paper, Kinetic Monte Carlo (KMC) simulation is applied to explore the formation of the passive SEI layer in the tangential direction of the lithium-ion intercalation in a graphite anode. The simulations are consistent with experimental observations that the active surface coverage decreases with time slowly in the initial stages of the battery operation, and then decreases rapidly. The effects of operating parameters such as the exchange current density, charging voltage, and temperature on the formation of the passive SEI layer are investigated. The active surface coverage at the end of each charging cycle remained constant for more cycles at higher temperature, but was lower at later cycles. The temperature that optimizes the active surface in a lithium-ion battery at cycle 1 can result in much lower active surface for most of the battery life. The potential for coupling the KMC model with porous electrode theory-continuum models is discussed to arrive at a multiscale model for understanding, analyzing, and minimizing capacity fade.
 [DOI: 10.1149/1.3548526] 

Manuscript submitted June 8, 2010; revised manuscript received January 5, 2011. Published February 14, 2011.

Rechargeable lithium-ion batteries have been extensively used in mobile communication and portable instruments due to their high volumetric and gravimetric energy density and low self-discharge rate. The lithium-ion battery is also promising for electric (plug-in and hybrid) vehicles and stationary energy storage applications, which has motivated many scientists and engineers to work toward developing lithium-ion batteries with improved performance and longer life.

The principal components of a typical lithium-ion battery are a carbonaceous anode, an organic electrolyte, and a transition metal-oxide cathode (such as $LiCoO_2$, $LiMn_2O_4$, or $LiNiO_2$). When a carbon electrode in a nonaqueous electrolyte is charged for the first time from the open-circuit potential, lithium ions are intercalated into a carbon structure. Along with Li-ion intercalation, other (electro)chemical reactions such as decomposition of the electrolyte and the formation of a surface layer occur. This surface layer is often referred as the solid-electrolyte-interface (SEI) layer. The properties and chemical composition of the SEI layer have been a subject of intense research due to its importance in the safety, capacity fade, and the life cycle of Li-ion secondary batteries.

The SEI layer is a key element of traditional Li-ion batteries and acts as a safety feature by maintaining a protective barrier between the negative electrode and the electrolyte. The SEI layer, which forms mainly in the first cycle of charging, should be thin, porous, and stable to provide a barrier between the electrolyte and electrode while allowing the passage of lithium ions. In some cycles during the life of the battery, the battery may be subjected to unwanted conditions such as overcharging, fragmenting, and short-circuiting, which leads to the formation of byproducts. These byproducts plate the pores in the SEI layer and increase its thickness, creating a passive SEI layer, which result in increasing the resistance to the intercalation/deintercalation of lithium ions and in turn results in reducing the capacity of the battery. These phenomena can increase temperature and lead to thermal runaway. The SEI layer should be highly ion-conductive to reduce overvoltage, while being mechanically stable and flexible. These objectives require a thin but stable SEI layer that will not deteriorate or substantially change its composition or morphology with time and temperature during cycling and storage. Understanding the mechanisms of formation, growth, and reduction of the passive SEI layer could be valuable if applied to the design of lithium-ion batteries with increased cyclability, safety, and life.

To understand the importance of capacity fade in a lithium-ion secondary battery system, significant efforts have been devoted to the development of mathematical models that describe the discharge behavior and formation of the active and passive SEI layers. The majority of these models are empirical or semiempirical,[1,2] which strongly depend on various empirical parameters fit to experimental data with limited predictive capability. Stamps et al.[3] proposed a hybrid estimation algorithm for analyzing capacity fade based on the assumption that parameters in a simple diffusion model drift slowly in between cycles; the model ignored limitations in the electrolyte phase. Arora et al.[4] simulated capacity fade by considering the lithium deposition as a side reaction during over-charge conditions and extended this modeling concept for increasing thickness of the surface film with cycling. Ramadass et al.[5] presented a semiempirical model for capacity fade that included the state of charge, solid-phase diffusion coefficient, and film resistance as a function of cycle number. Capacity fade was estimated by either accounting for active material loss or rate capacity loss. State of charge of the limiting electrodes accounted for the active material loss. The effective diffusion coefficient of the limiting electrodes was the parameter used to account for the rate capacity loss during the cycling.[6] Ramadass et al.[7] studied capacity fade for spinel-based lithium-ion batteries through incorporation of side reactions in the lithium-ion intercalation model. Their model assumed that the loss of the active materials with continuous cycling was attributed to a continuous film formation over the surface of the negative electrode. The model indicated that, over time, the active SEI layer becomes stable while resistance increases due to the formation of the passive SEI layer. Ploehn et al.[8] presented a first-principles model of solvent diffusion describing the growth of a passive SEI layer. The model assumes that solvent reduction produces an insoluble product that contributes to the growth of a passive SEI layer. Their results indicate that the passive SEI layer thickness increases with the square root of time. Their findings suggest that the initial formation of a 10–100 nm thick passive SEI layer can accompany a 10–20% initial capacity loss. Zhang and White[9] considered that the major mechanisms for capacity fade are the loss of lithium ions by a film formation reaction and loss of active material in the cathode.

Bhattacharya and Van der Ven[10] performed a first-principles investigation of the concentration-dependent Li-diffusion coefficient in spinel $Li_{1+x}Ti_2O_4$ using the Kinetic Monte Carlo (KMC) simulation model proposed by Bortz et al.[11] They concluded that the

* Electrochemical Society Student Member.
** Electrochemical Society Active Member.
z E-mail: vsubramanian@seas.wustl.edu

octahedral sites are activated states for Li hops between neighboring tetrahedral sites for low lithium concentration, and that the migration barrier decreased with increased lithium concentration. The authors also provided insights into the effect of crystallographic features in spinel and layered intercalation compounds on Li mobility. First-principles investigations of lithium diffusion within the layer form of $Li_xCoO_2$ were explored by Van der Ven and Cedar[12] using a KMC simulation for predicting the lithium diffusion through a deviancy mechanism for low to high concentration of lithium with isolated vacancy dilution. They concluded that for various concentrations of lithium, migration to the adjacent vacant octahedral sites is governed by a divacancy mechanism and the migration path of this mechanism passes through a tetrahedral site. They also concluded that the activation barrier associated with the divacancy hop mechanism increases with decreasing concentration of lithium. Van der Ven et al.[13] studied diffusion of Li in $Li_xTiS_2$ for various lithium-ion concentrations using a mixed-basis cluster expansion approach. They analyzed the collective transport in concentrated intercalation compounds using atomic-scale energies to parameterize the cluster expansion Hamiltonian function, which then was used in thermodynamic and kinetic (Monte Carlo) simulations. They used the Monte Carlo algorithm proposed by Bortz et al.[11] with $12 \times 12 \times 12$ Li sites. The Monte Carlo simulation used 1000 passes, where each pass corresponded to as many Li hops as there are Li sites. They postulated that the migration barriers for Li hops are very sensitive to the local environment with a lower migration barrier occurring when Li hops into a divacancy as opposed to an isolated Li vacancy. Wagemaker et al.[14] studied the thermodynamic and structural properties of $Li_xTiO_2$ spinel using a cluster expansion based on pseudo-potential ground-state energy calculations in the generalized gradient approximation. Monte Carlo simulation was used to predict the configuration space and predict thermodynamic quantities. Their Monte Carlo cell contained 10,368 Li sites with 6000 Monte Carlo passes per lattice site for each chemical potential and temperature step.

The novel contribution of this paper, compared to published Monte Carlo simulations, is that surface heterogeneity is explicitly addressed. This enables an exploration of passive SEI layer formation and capacity fade. Many mathematical models in the literature attempt to predict capacity fade caused by growth of the passive SEI layer in only one direction: along the intercalation of Li ions. These models are not able to predict growth and formation of the passive SEI layer across the surface of the electrode particles (at the interface of the electrode and electrolyte). It is reported in literature that the formation and growth of the passive SEI layer takes place around the electrode particle while intercalating $Li^+$ in the electrode particles.[15] The effect of increasing the passive SEI layer thickness along the direction of the intercalation/deintercalation will negligibly affect the performance of the battery as compared with increasing the coverage across the surface of the interface. Continuum models do not account for this surface heterogeneity across the surface of the electrode, which is explored in this paper using KMC simulation.

There are several contributions to the capacity fade of lithium-ion batteries, including agglomeration, stress-related expansion, inter-dendritic cavity defects, phase changes, and increase in the thickness of the passive SEI layer.[9] The objective of this paper is to apply KMC simulation to investigate the formation and growth of the passive SEI layer, especially in the area tangential to the surface of the anode during charging and discharging cycles of lithium-ion battery. The thickness of the passive SEI layer is affected by many mechanisms such as byproduct formation, thermal runaway, and stresses in the electrodes. This paper considers the side reaction mechanism for the formation of passive SEI layer. Lithium-ion batteries exhibit capacity fade with cycles, which requires modeling at the system level (charge–discharge curves). The growth of the passive SEI layer on the order of few nanometers at the anode and irreversible capacity losses due to side reactions which occur at the molecular level are responsible for the nonidealities in the behavior of lithium-ion batteries. Hence, formation and growth of the passive SEI layer is best modeled with molecular simulations, making KMC a more appropriate simulation method than continuum approaches.

## Kinetic Monte Carlo Model

In general, it is assumed that the Li-ions generated by the electrochemical reaction will move from anode to cathode or vice versa, depending on discharge or charge mode given as

$$CoO_2 + Li^+ + e^- \underset{\text{Charge}}{\overset{\text{Discharge}}{\rightleftharpoons}} LiCoO_2 \text{ at cathode} \quad [1]$$

$$LiC_6 \underset{\text{Charge}}{\overset{\text{Discharge}}{\rightleftharpoons}} Li^+ + e^- + C_6 \text{ at Anode} \quad [2]$$

When the Li-ion reacts with the particles of the electrode in charging mode, the formation of undesired product occurs according to a side reaction such as (S = Surface)

$$S + 2Li^+ + 2e^- \rightarrow P \quad [3]$$

The undesired product (P) contributes to either increasing the thickness of the passive SEI layer or blocking the pores of the existing stable active porous SEI layer, which increases the internal resistance and decreases the rate of intercalation/deintercalation. Capacity fade is generally associated with the decrease in the rate of intercalation/deintercalation.

KMC is used to simulate the phenomena that take place on the surface of the interface of the battery during the charging cycles. The paper considers a single electrode surface (negative electrode) and phenomena such as adsorption, desorption, surface diffusion, and formation of passive material that blocks the pores of the active SEI layer and increases the coverage of the passive SEI layer. Desorption and surface diffusion are related with a stable and porous active SEI layer whereas adsorption and formation of passive materials are related with growth of the passive SEI layer. Formation and growth of the passive SEI layer is considered as a side reaction represented by using the Butler–Volmer equation. This equation considers the mechanisms of forward and backward reactions.[7] Lithium ions are intercalated on the anode surface during the charging mode of the battery. This phenomenon can be viewed as the adsorption and formation of passive materials over the electrode surface in the electrochemical reaction. Deintercalation takes place at the anode during discharging of the battery. This phenomenon can be viewed as desorption of materials from the electrode surface in the electrochemical reaction. The rate of diffusion of molecules on the surface during electrochemical reactions is modeled using a cubic lattice.[15] The intercalation of $Li^+$ from electrolyte to the electrode can be described by[16]

$$\text{Adsorption rate: } K_1 C_{Li^+}^{0.5} \exp(-\alpha F \eta / RT) \quad [4]$$

The adsorbed Li (see Fig. 1) can intercalate inside or diffuse on the electrode surface or form a passive layer. The liberation of Li from the electrode particle is described by[15]

$$\text{Desorption rate: } K_2 C_{Li^+}^{0.5} \exp(\alpha F \eta / RT) \quad [5]$$

where the nonlinear reaction rate constants $K_1$ and $K_2$ are functions of the active surface coverage $\theta$, and are given by

$$K_1 = \frac{3}{R_{pn}} k_n (1 - \theta) \quad [6]$$

$$K_2 = \frac{3}{R_{pn}} k_n \theta \quad [7]$$

The value of $k_n$ (electrochemical rate constant typically used in the continuum model) is shown in Table I and $\eta$ is the overpotential given by

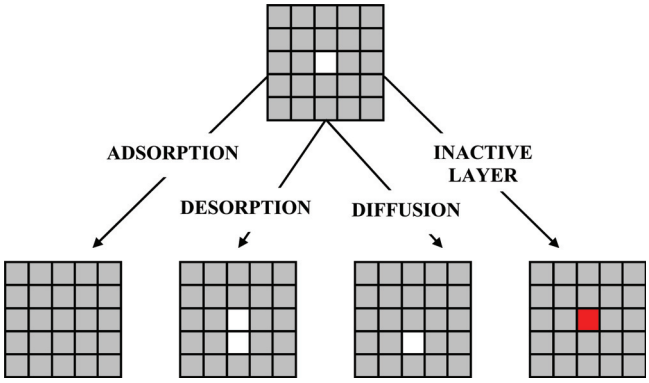


**Figure 1.** (Color online) Schematic representation of the phenomena represented in the KMC simulations.

$$\eta = V - U_n \quad [8]$$

with $V$ being the applied voltage with respect to graphite (lower voltages results in a faster rate of charge), and the open-circuit potential $U_n$ given by

$$U_n = 0.7222 + 0.1387\theta + 0.029\theta^{0.5} - \frac{0.0172}{\theta} + \frac{1.9 \times 10^{-3}}{\theta^{1.5}} + 0.2808\exp(0.9 - 15\theta) - 0.7984\exp(0.4465\theta - 0.4108) \quad [9]$$

Other important rates are given by[15]

$$\text{Surface diffusion rate: } \frac{1}{2}\gamma_D\theta(1-\theta). \quad [10]$$

$$\text{Passive SEI layer formation rate: } K_3\exp(-0.5F(V - U_{n_{SEI}})/RT) \quad [11]$$

where $K_3$ is a function of the exchange current density typically used in the continuum model and is given by

$$K_3 = \frac{3}{R_{pn}F}i_{0,P} \quad [12]$$

The formation of the passive SEI layer is assumed to be governed by Butler–Volmer kinetics, as shown in Eq. 11. The term $(V - U_{n_{SEI}})$ indicates the overpotential for SEI layer.

A surface KMC simulation was implemented in which the transition rates from one configuration of the lattice sites to other configurations were computed from Eqs. 4 to 12 in the standard way, with acceptable transitions as shown in Fig. 1 (Ref. 17; see Table I for the list of parameters).[17] The electrode surface was described by a $25 \times 25$ molecule mesh for a total of 625 sites (increasing the lattice size did not change the results significantly). Lithium metal formed at a site is assumed to intercalate instantaneously. The total number of lithium ions was given by the electrolyte concentration (1 M). At each KMC step, all possible transitions out of the current configuration are considered, along with their corresponding transition rates, and the new configuration $r$ is selected that satisfies the inequality

$$\frac{\sum_{j=0}^{r-1} k_j}{\sum_{j=0}^{N} k_j} \leq \chi_1 < \frac{\sum_{j=0}^{r} k_j}{\sum_{j=0}^{N} k_j} \quad [13]$$

where $k_j$ is the $j$th transition rate and $\chi_1$ is a uniformly distributed random number between 0 and 1. The probability of a transition selected from Eq. 13 is proportional to its transition rate. The KMC time step was calculated according to[18]

$$\Delta t = -\frac{\ln \chi_2}{\sum_{j=0}^{N} k_j} \quad [14]$$

where $\chi_2$ is a uniformly distributed random number between 0 and 1 and $\Delta t$ is the time between transitions, typically ranging from on the order of $10^{-9}$ s for the first step to 0.1 or 1 s for the final time steps. The high rates of charging in the initial stages of charging cause very high rates of adsorption of the active layer at early times, and, therefore, very short time steps. As the charging progresses, the open-circuit potential decreases. This decrease occurs drastically during the first few steps due to the $1/\theta$ term in Eq. 9. Equation 4 shows that the rate of adsorption has an exponential dependence on the open-circuit potential. Therefore, the adsorption rate decreases by several orders of magnitude in a short time. The rates for the other possible transitions do not become significant until higher surface coverage, and do not reach the high rates achieved during the initial adsorption.

Once a given event is selected, the transition to the new configuration $r$ was executed, and the entire process was repeated. This KMC model simulates passive SEI layer formation, reduction, and growth in lithium-ion secondary batteries including in the perpendicular direction of the lithium-ion intercalation (tangential to the surface). Molecules of the same type are assumed to have an affinity for each other on the surface, with the probability of a passive

**Table I. Parameter values used in the KMC simulation.**

| | Parameters | Values | Reference |
|---|---|---|---|
| $a_n$ | Specific surface area of the negative electrode, $m^2/m^3$ | 723,600 | 24 |
| $ct_n$ | Electrolyte concentration, $mol/m^3$ | 30,555 | 24 |
| $D_{sn}$ | Lithium-ion diffusion coefficient in the intercalation of negative electrode, $m^2/s$ | $3.9 \times 10^{-14}$ | 24 |
| $F$ | Faraday's constant, C/mol | 96,487 | |
| $i_{0,P}$ | Exchange current density, $A/m^2$ | $1.5 \times 10^{-9}$ | 5 |
| $k_n$ | Intercalation/deintercalation reaction rate constant, $(mol/m)^{0.5}/s$ | $5.0307 \times 10^{-11}$ | 24 |
| $l_n$ | Thickness of negative electrode, m | $8.8 \times 10^{-5}$ | 24 |
| $R$ | Universal gas constant, J/(mol K) | 8.314 | |
| $R_{pn}$ | Radius of intercalation of negative electrode, m | $2 \times 10^{-6}$ | 24 |
| $T$ | Operating temperature, K | 303.15 | |
| $U_n$ | Open-circuit potential of the negative electrode, V | | 24 |
| $U_{n_{SEI}}$ | Open-circuit potential of the SEI layer, V | 0.4 | 15 |
| $V$ | Applied potential with respect to graphite (equivalent to $4.2 - 0.001 = 4.199$ V for a lithium-ion battery with the cathode operating at 4.2 V with no limitations) | 0.001 | |
| $\gamma_D$ | Diffusion frequency, 1/s | $1 \times 10^{-10}$ | 24 |

molecule forming on a site being twice as high when a passive molecule is at a neighboring site. This model for the affinity of like molecules on surfaces is similar to that used in past KMC models for electrochemical systems.[16,17] This simulation was continued until the electrode is fully charged or a time cutoff of 1000 s was reached. The number of KMC steps in each simulation depended heavily on the cycle number and the buildup of the passive SEI layer, and ranged from several hundred to over 10 000 moves per cycle.

The charging cycle of a lithium-ion battery was assumed to be under constant potential. Simulation under constant current operation is more computationally challenging, but can be implemented using the same KMC model. All simulations in this work were implemented in Maple13/MATLAB (Refs. 19 and 20) with an in-house KMC code using a personal computer with a 2.4 GHz processor and 2 GB of RAM. The results are obtained for first 100 cycles of charging. During the beginning of every charging cycle, the particle is assumed to be completely discharged. The surface coverage of passive molecules in the SEI layer was estimated from the end of the previous cycle of charging and the surface coverage of active atoms was estimated using Faraday's law for discharge, which means that all the intercalated lithium comes out during discharge. A flowchart of the calculations that occur in a single KMC step is shown in Fig. 2. The kinetic parameters and reaction schemes are obtained from continuum models and following procedures are described by Drews et al.[21]

## Results and Discussion

For the first charging cycle of the simulation, the active surface coverage (ratio of numbers of molecules of active SEI layer to the total number of molecules on the anode surface) was observed to increase with time, reaching nearly a steady-state value in ~178 s (see Fig. 3). The rate of growth of active surface is high initially and slowly decreases. Figure 4 show the active surface coverage for various charging cycles. The steady-state active surface coverage is observed to decrease with increasing cycle number. The initial rate of formation of active surface is similar in each cycle, with the time to reach steady-state decreasing with increasing cycle number. The decrease in the active surface coverage is due to the formation of the passive SEI layer on the surface in the tangential direction to the

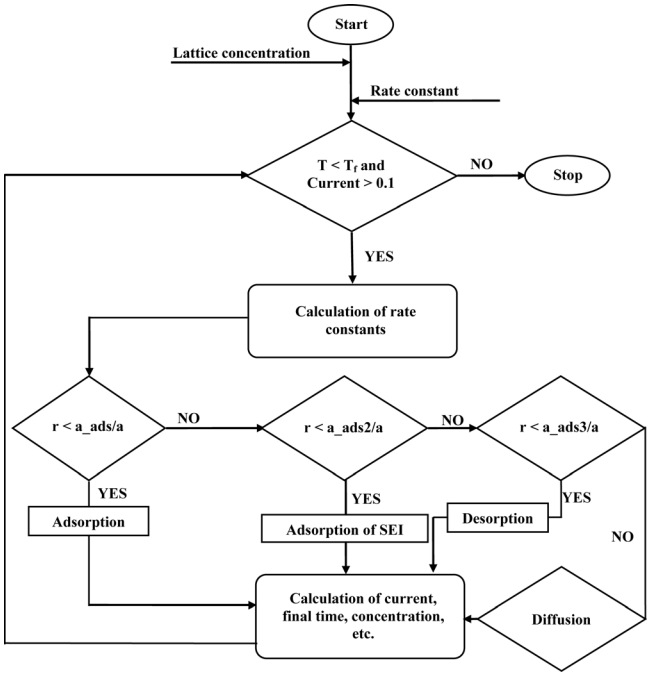


**Figure 2.** Flowchart of calculations in a single KMC step.

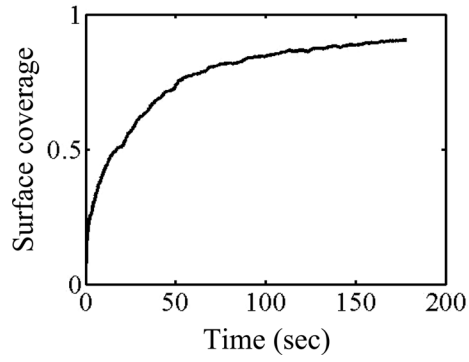


**Figure 3.** Time variation of the active surface coverage during the first charging cycle. A steady-state value of 178 s was computed as the time taken to reach 99% of its final constant value.

lithium-ion intercalation. The time required for charging decreases with the number of cycles (see Fig. 4) due to the growth of the passive SEI layer and the reduced surface area available for the electrodeposition of active atoms and reduced capacity. Figure 5 more clearly illustrates the dominant dynamics occurring during charging. The time scales of variation in the active surface coverage range from 0.01 to 100 s. These results suggest that the simulation time may be reduced by applying a quasi-steady-state assumption and solving the system within aforementioned time scales only, which is an approach that has been applied in KMC simulations of other electrochemical processes.[22,23]

The active surface coverage at the end of each charging cycle is plotted with the number of charging cycles in Fig. 6. An interesting observation is that the active surface coverage remains constant for the initial ~10 charging cycles, that is, the capacity of the lithium-ion battery does not fade for the initial cycles of charging. After this initial period, the active surface coverage decreases with cycle number and the battery capacity reduces with number of charging cycles. This behavior is consistent with observations of capacity fade in real batteries. It is generally observed experimentally that the active surface coverage decreases with time slowly in the initial stages of the battery operation, and then decreases rapidly.[3–9] As a battery undergoes several charging and discharging cycles, the amount of passive SEI layer on the surface becomes substantial, and less active surface area is available. This leads to a greater resistance to intercalation and deintercalation of the lithium ions and the rate of charging/discharging drops significantly. More unwanted byproducts are formed, and active surface coverage decreases rapidly in the middle to latter stages of the battery life cycle. These experimental observations agree with the KMC simulation results in Fig. 6.

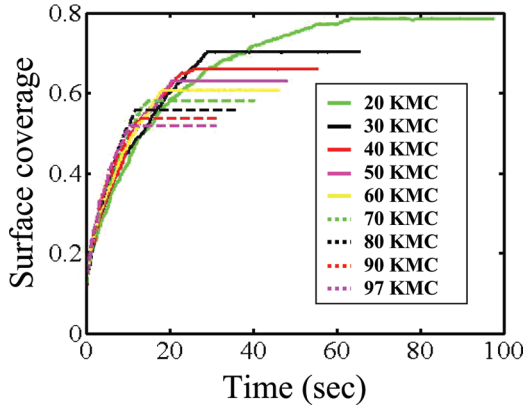


**Figure 4.** (Color online) Time variation of the active surface coverage for different cycles up to steady state. One cycle corresponds to charging and discharging at a very high rate (Voltage = 4.2 V – 0.001 V = 4.199 V).

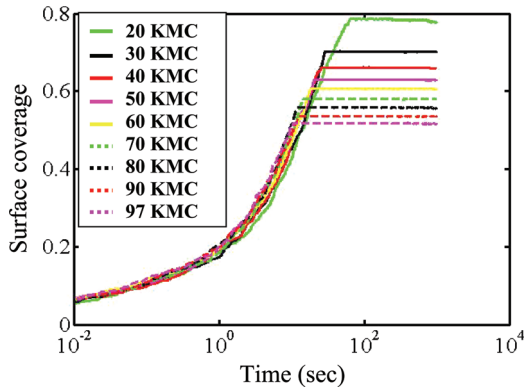


**Figure 5.** (Color online) Time variation of the active surface coverage for various charging cycles illustrating dominant dynamics.

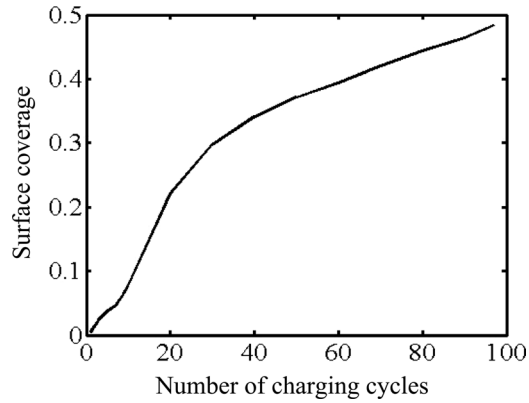


**Figure 7.** Time variation of the final SEI surface coverage at various charging cycles.

Figure 7 is a plot of the surface coverage of the passive SEI layer at the end of each charging cycle with number of charging cycles. The rate of formation of the passive SEI layer is initially high and reduces in latter cycles of charging. The short-time behavior of the initial charging involves the rapid formation of the first few molecules of the passive SEI layer. Although the formation of molecules of the passive SEI layer is faster initially, its concentration is not significant enough to cause capacity fade of the battery and capacity loss of the battery is not observed during the first few cycles of charging. Figures 8 and 9 show the initial and final morphology of the surface of the anode. In the first cycle of charging, the passive SEI layer molecules are scattered on the surface. In the final surface structure, the passive SEI layer is formed in clusters. In this simulation, the initial surface coverage of active sites was kept at a constant value before starting the KMC simulation.

Researchers have investigated the effect of various operating parameters on the formation of the passive SEI layer.[3–9] The effect of the exchange current density ($i_0$) and temperature ($T$) on the evolution of the active and passive surface of SEI layer coverages for the KMC model are shown in Figs. 10 and 11. The processes of formation of the active and passive SEI layer are a function of temperature as shown in Eqs. 4–7. The effect of temperature was investigated by varying the temperature while keeping all other parameters at the base conditions. The active surface coverage under the fully charged condition remained constant for the lower exchange current density of $1.5 \times 10^{-10}$ A/m$^2$ (see Fig. 10). For an exchange current density of $1.5 \times 10^{-9}$ A/m$^2$, the active surface coverage under fully charged conditions was initially somewhat lower for the higher temperature of 320 K, but maintained a higher value for all subsequent cycles. These results indicate that the temperature that optimizes the initial active surface coverage in a lithium-ion battery at early cycles can result in much lower active surface coverage for most of the battery life. The coverage of the passive SEI layer is less at lower exchange current density and higher temperature (see Fig. 11). It is very desirable to decrease the growth rate of molecules in the passive SEI layer which will block the pores of the stable SEI layer; on the other hand, it is not desirable to increase the temperature of the lithium-ion battery above certain values, for safety and mechanical reasons. The effect of the exchange current density on the morphology of the lattice of the electrode is observed by comparing Figs. 8, 9, 12, and 13. The coverage of the passive SEI layer (red color sites on the lattice) is lower for lower exchange current density, keeping temperature and all other parameters at the base values. The rate of formation of passive SEI layer sites is proportional to the exchange current density, such that a decrease in the exchange current density results in a decrease in the formation of the passive SEI layer. In the base case, the passive SEI layer is observed to be in the form of clusters with the longest chain containing 17 sites connected with each other (Fig. 9) whereas with lower exchange current density the clusters are small and scattered with only two sites connected with each other (Fig. 13). Approximately 48% of the lattice sites are covered for the base case compared to 6.55% for the reduced exchange current density.

This type of data and analysis could assist in the prediction of the value of the exchange current density based on the total time required for the battery to encounter failure, assuming that passive layer formation is the cause of failure. The simulations were carried out at high applied potential for charging (equivalent to high currents). This paper only examines a constant potential charging

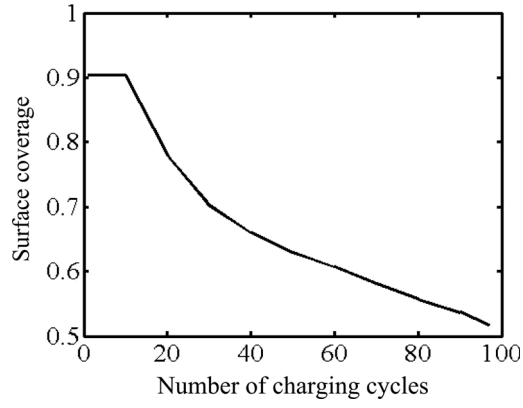


**Figure 6.** Time variation of the final active surface coverage at various charging cycles.

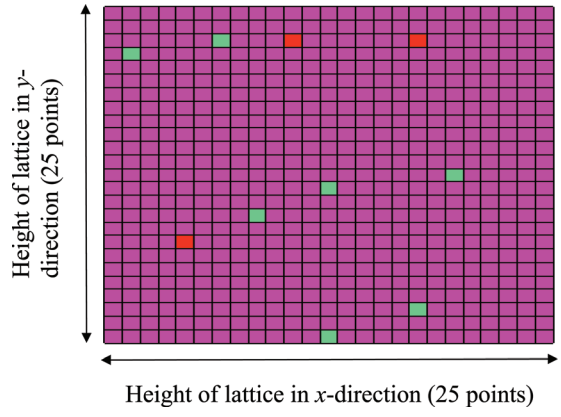


**Figure 8.** (Color online) Initial lattice configuration of the first cycle: Magenta represents virgin sites, Red represents sites with passive SEI layer, and Green represents absorbed lithium sites. Exchange current density $i_0 = 1.5 \times 10^{-9}$ A/m$^2$.

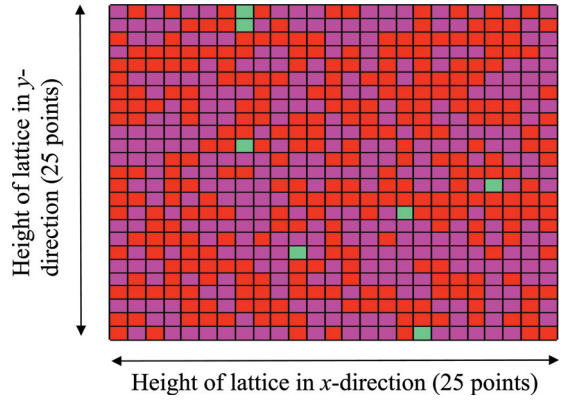


**Figure 9.** (Color online) Final lattice configuration of the last cycle: Magenta represents virgin sites, Red represents sites with passive SEI layer, and Green represents absorbed lithium sites. Exchange current density $i_0 = 1.5 \times 10^{-9}$ A/m$^2$.

protocol, rather than a constant current followed by constant potential protocol. This results in a much higher charging rate during the initial seconds of any charging cycle, which tapers to zero as the battery becomes fully charged. Future work will incorporate a constant current charging protocol. Constant potential is easy to implement because the same potential is applied for main reaction and the side reaction (more like two resistors in parallel). However, constant current involves individual current for the main and side reactions changing with time and the state of charge. Due to the high rates of charging, the time required for charging and the simulation time was reduced, however, the electrode fails in nearly 100 cycles. Low rates of charging would make the KMC simulations highly computationally expensive. High rates of charging will enhance the rate of intercalation as well as deintercalation, which results in high rate of byproduct formation. If the byproduct formation rate is high, then the surface coverage of the passive SEI layer will be high and capacity fade will occur at the faster rate and life cycle of the battery will reduce significantly. To make the simulations efficient, some of the important aspects like mass transfer in the electrolyte and Ohmic limitations were ignored, which are important at high rates of charging. In the future, the KMC model will be coupled with reduced order models for the continuum phases to perform multiscale simulations for a wide range of operating conditions.

Additionally, the effect of charging potential on the surface coverage composition was examined. Figure 14 shows the end-of-charge active surface coverage for various applied potentials. The

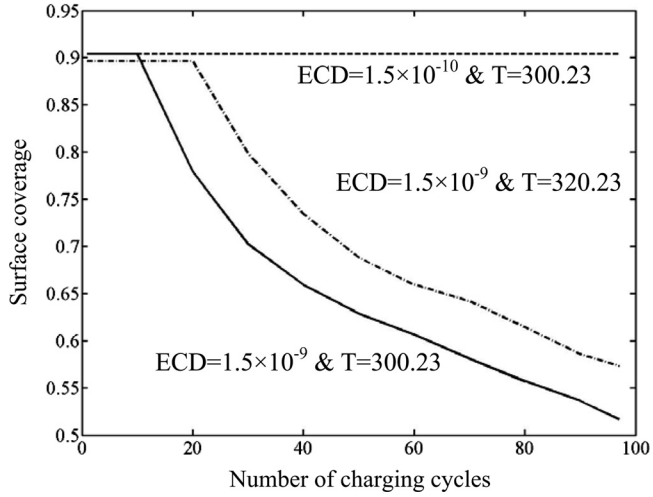


**Figure 10.** Effect of exchange current density and temperature on the depletion of active surface coverage (ECD = exchange current density).

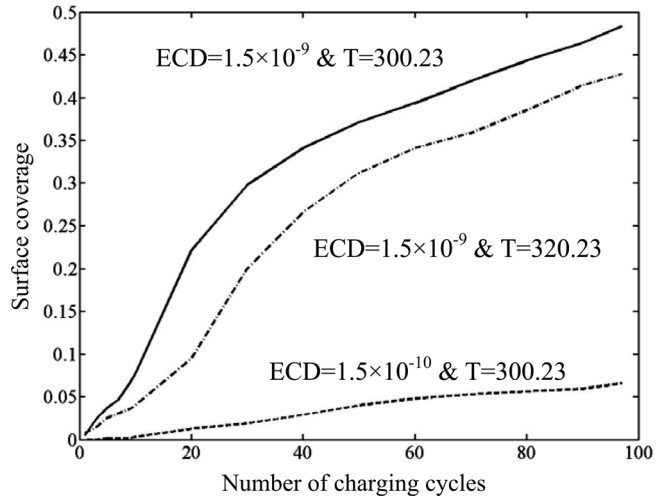


**Figure 11.** Effect of exchange current density and temperature on the growth of the SEI layer in a Li-ion battery (ECD = exchange current density).

simulations predict that the life of a battery increases for a higher applied potential versus graphite, which is equivalent to a lower charging voltage. For all charging potentials, no change in active surface coverage is observed for the first several cycles. The number of cycles that are run before a change in the active surface coverage is observed based on the rate of charge. This ranges from about ten cycles for high rates of charging to hundreds or thousands for lower rates of charging. For lower charging rates, the active surface coverage is predicted to be much less in the initial cycles than with the higher rates. This is expected if we are charging a constant low potential, because the battery is not charged to 4.2 V, as is typical for Li-ion batteries. If the battery is charged only to 4 V or less, the battery has a large amount of unused capacity that is reflected in the maximum active surface coverage.

Similarly, the growth of the passive layer with cycle number is shown in Fig. 15. The KMC results indicate that the rate of increase of the passive layer is approximately linear during the first charge cycles. This linear region corresponds to the cycles in which the active surface coverage does not change (Fig. 14). Once the passive surface coverage reaches a critical value, the KMC results indicate that the maximum active surface coverage begins to decrease while the passive layer grows at an increased rate. The growth of the passive layer then begins to taper until the battery fails. As would be expected, lower rates of charging results in a lower initial growth

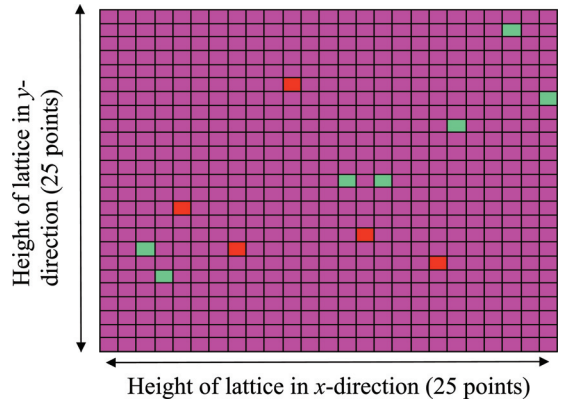


**Figure 12.** (Color online) Initial lattice configuration of the first cycle: Magenta represents virgin sites, Red represents sites with passive SEI layer, and Green represents absorbed lithium sites. Exchange current density $i_0 = 1.5 \times 10^{-10}$A/m$^2$.

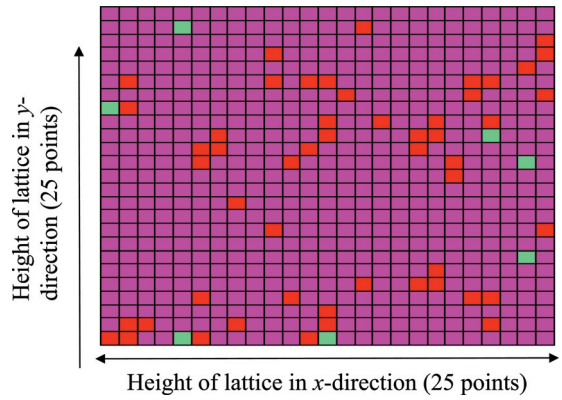


**Figure 13.** (Color online) Final lattice configuration of the last cycle with decreasing red sites compared with Fig. 9: Magenta represents virgin sites, Red represents sites with passive SEI layer, and Green represents absorbed lithium sites. Exchange current density $i_0 = 1.5 \times 10^{-10} \mathrm{A/m^2}$.

rate of the passive layer, which allows the battery to be operated for more cycles. An interesting observation is that, once the critical passive layer coverage is reached, the rate of the passive layer growth is similar for all applied potentials. Another interesting observation is that the lower changing rates can actually reach a higher surface coverage of the passive layer before a failure mode is reached. Because less of the surface is required for the active layer sites when charging to a lower battery voltage (higher applied potential versus graphite), more sites can be disabled before an effect is noticed on the steady-state active surface coverage at the end of each cycle.

## Conclusions

Prediction of capacity fade in lithium-ion secondary batteries is a challenging research problem. The literature[3–6] reports that the formation and growth of a passive SEI layer is mainly responsible for capacity fade in a lithium-ion secondary battery. Passive SEI layer formation is modeled in this paper using a Kinetic Monte Carlo simulation. The simulation results are in good agreement with observations reported in literature for the passive SEI layer. It was observed that the active surface coverage remains constant for the initial charging cycles and then decreases monotonically with number of charging cycles. It was also observed that the rate of formation of passive SEI layer sites was high for the initial few cycles, but the amount of molecules were not significant enough to affect the capacity fade of the battery during the initial cycles of charging.

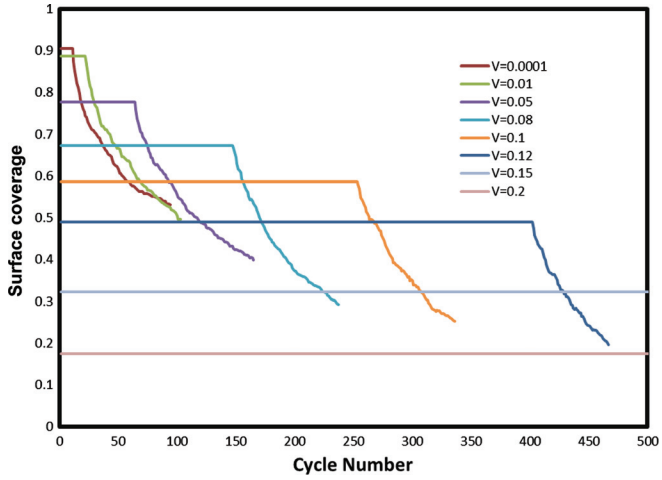


**Figure 14.** (Color online) End of cycle active surface coverage for various charging potentials.

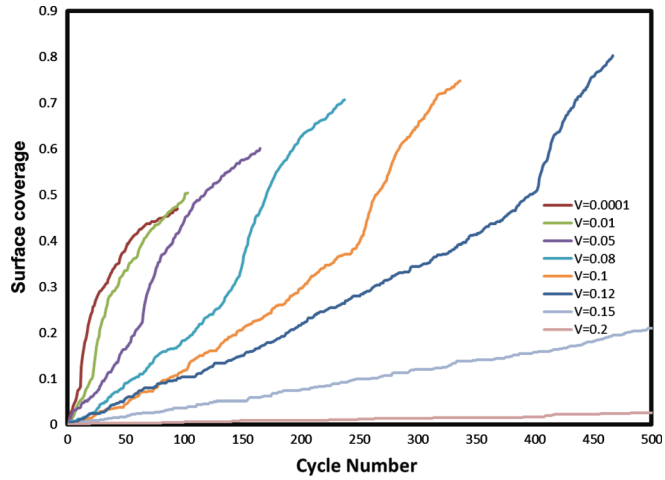


**Figure 15.** (Color online) End of cycle passive surface coverage for various charging potentials.

The KMC simulations were able to simulate the formation of a passive SEI layer and subsequently the capacity fade of the lithium-ion battery. The coverage of the passive SEI layer was less at lower exchange current density, as expected. Based on the simulation parameters, higher temperature favors the main reaction (Eqs. 1 and 2) compared to the formation of the passive layer. However, this relationship may change depending on the electrolyte and chemistry. An optimal temperature may exist for minimizing the passive layer formation and minimizing the material loss at high temperatures. In addition, the dependence of rate constants/exchange current on the temperature needs to be included to quantify the effect of temperature with reasonable confidence.

The effect of different charging potentials also behaved as anticipated, as lower rates of charge resulted in slower growth of the passive SEI layer and longer battery life. Unfortunately, charging at such low voltages ensures the battery will be heavily underutilized. This can be improved by a constant current charge followed by a constant potential charge. A KMC simulation implementing such a charging protocol would be more complicated to implement but would prevent the rapid degradation observed in this paper.

A natural next step is to dynamically couple the KMC model with continuum models for the electrolyte and solid phase. One approach would be to apply a coupled KMC-continuum simulation to the charging process, to predict the formation of the passive SEI layer, with discharging described by a purely continuum model. Such multiscale model may enable the prediction of the formation, growth, and reduction of the passive SEI layer as well as the analysis of capacity fade. The computational cost of the continuum models can be reduced by using a recently published reformulated pseudo-two dimensional (2D) model.[24]

## Acknowledgments

The authors are thankful for the partial financial support of this work by the Institute for Advanced Computing Applications and Technologies, the National Science Foundation under contract numbers CBET-0828002, CBET-0828123, and CBET-1008692, the International Center for Advanced Renewable Energy and Sustainability at Washington University in St. Louis, (ICARES), and the U.S. government.

*Washington University assisted in meeting the publication costs of this article.*

## References

1. B. Bloom, J. Cole, S. Sohn, E. Jones, V. Polzin, G. Battaglia, C. Henriksen, R. Richardson, T. Unkelhaeuser, D. Ingersoll, et al., *J. Power Sources*, **101**, 238 (2001).
2. B. Liuaw, R. Jungst, G. Nagasubramanian, H. Case, and D. Doughty, *J. Power Sources*, **140**, 157 (2005).

3. A. T. Stamps, C. E. Holland, R. E. White, and E. P. Gatzke, *J. Power Sources*, **150**, 229 (2005).
4. P. Arora, B. N. Popov, B. Haran, M. Ramasubramanian, S. Popova, and R. E. White, *Corros. Sci.*, **39**, 739 (1997).
5. S. Santhanagopalan, Q. Guo, P. Ramadass, and R. E. White, *J. Power Sources*, **156**, 620 (2006).
6. V. Ramadesigan, V. Boovaragavan, M. Arabandi, K. Chen, H. Tuskamoto, R. D. Braatz, and V. R. Subramanian, *ECS Trans.*, **19**(16), 11 (2009).
7. P. Ramadass, P. M. Gomadam, R. E. White, and B. N. Popov, *J. Electrochem. Soc.*, **151**, A196 (2004).
8. H. Ploehn, P. Ramadass, and R. White, *J. Electrochem. Soc.*, **151**, A456 (2004).
9. Q. Zhang and R. White, *J. Power Sources*, **179**, 793 (2008).
10. J. Bhattacharya and A. Van der Ven, *Phys. Rev. B*, **81**, 104304 (2010).
11. A. B. Bortz, M. H. Kalos, and L. Lebowitz, *J. Comput. Phys.*, **17**, 10 (1975).
12. A. Van der Ven and G. Cedar, *Electrochem. Solid-State Lett.*, **3**, 301 (2000).
13. A. Van der Ven, J. C. Thomas, Q. Xu, B. Swoboda, and D. Morgan, *Phys. Rev. B*, **78**, 104306 (2008).
14. M. Wagemaker, A. Van der Ven, D. Morgan, G. Cedar, F. M. Mulder, and G. J. Kearley, *Chem. Phys.*, **317**, 130 (2005).
15. G. Sikha, B. N. Popov, and R. E. White, *J. Electrochem. Soc.*, **151**, A1104 (2004).
16. T. O. Drews, A. Radisic, J. Erlebacher, R. D. Braatz, P. C. Searson, and R. C. Alkire, *J. Electrochem. Soc.*, **153**, C434 (2006).
17. T. O. Drews, R. D. Braatz, and R. C. Alkire, *Z. Phys. Chem.*, **221**, 1 (2007).
18. K. Fichthorn and W. H. Weinberg, *J. Chem. Phys.*, **95**, 1090 (1991).
19. http://www.mathworks.com, last accessed: May 10, 2010.
20. http://www.maplesoft.com/Products/Maple, last accessed: May 10, 2010.
21. T. O. Drews, R. D. Braatz, and R. C. Alkire, *Int. J. Multiscale Comp. Eng.*, **2**, 327 (2004).
22. Z. Zheng, R. Stephens, R. D. Braatz, R. C. Alkire, and L. R. Petzold, *J. Comput. Phys.*, **227**, 5184 (2008).
23. T. O. Drews, E. G. Webb, D. L. Ma, J. Alameda, R. D. Braatz, and R. C. Alkire, *AIChE J.*, **50**, 226 (2004).
24. V. R. Subramanian, V. Boovaragavan V. Ramadesigan, and M. Arabandi, *J. Electrochem. Soc.*, **156**, A260 (2009).